Talanta 140 (2015) 176–182

Contents lists available at ScienceDirect

Talanta

journal homepage: www.elsevier.com/locate/talanta

Establishment of a finite element model for extracting chemical reaction kinetics in a micro-flow injection system with high throughput sampling

Zeng-Qiang Wu [a], Wen-Bin Du [b,1], Jin-Yi Li [a], Xing-Hua Xia [a,*], Qun Fang [b,**]

[a] State Key Laboratory of Analytical Chemistry for Life Science, School of Chemistry and Chemical Engineering, Nanjing University, Collaborative Innovation Center of Chemistry for Life Sciences, Nanjing 210093, China
[b] Institute of Microanalytical Systems, Department of Chemistry, Zhejiang University, Hangzhou 310058, China

ARTICLE INFO

Article history:
Received 16 January 2015
Received in revised form
16 March 2015
Accepted 24 March 2015
Available online 1 April 2015

Keywords:
Diffusion
Micro-flow injection system
Finite element model
Reaction kinetics
Taylor dispersion

ABSTRACT

Numerical simulation can provide valuable insights for complex microfluidic phenomena coupling mixing and diffusion processes. Herein, a novel finite element model (FEM) has been established to extract chemical reaction kinetics in a microfluidic flow injection analysis (micro-FIA) system using high throughput sample introduction. To reduce the computation burden, the finite element mesh generation is performed with different scales based on the different geometric sizes of micro-FIA. In order to study the contribution of chemical reaction kinetics under non-equilibrium condition, a pseudo-first-order chemical kinetics equation is adopted in the numerical simulations. The effect of reactants diffusion on reaction products is evaluated, and the results demonstrate that the Taylor dispersion plays a determining role in the micro-FIA system. In addition, the effects of flow velocity and injection volume on the reaction product are also simulated. The simulated results agree well with the ones from experiments. Although gravity driven flow is used to the numerical model in the present study, the FEM model also can be applied into the systems with other driving forces such as pressure. Therefore, the established FEM model will facilitate the understanding of reaction mechanism in micro-FIA systems and help us to optimize the manifold of micro-FIA systems.

1. Introduction

Flow injection analysis (FIA) has been widely applied in analytical chemistry since it was introduced in 1975 [1]. Contrary to the conventional concept that chemical analysis relies on steady-state reactions, FIA provides a new way to exploit both physical and chemical processes under non-equilibrium conditions with reproducible operation timing. In addition, FIA can easily achieve automated operation with inexpensive instruments, which effectively makes it as a useful approach in practical applications. FIA has underg one great development with three main generations including FIA (the first generation), sequential injection analysis (SIA, the second generation) [2] and bead-injection (BI)-lab-on-valve (LOV) [3] (the third generation). The main driving force of these progresses is to miniaturize the manifolds for reducing the consumption of samples and reagents in FIA systems. Recently, with the development of micro-total analysis system (μTAS), an advanced generation of micro-FIA systems has been proposed to integrate the complex chemical manipulations and detection. In the early stage of the micro-FIA system, continuous flow model was usually used for bio-analysis [4], synthesis [5,6], sample purification [7] and extraction [8]. However, these devices encountered main disadvantages of significant consumption of reagents and cross-contamination. In order to overcome these problems, zone injection model using micro-pump and micro-valve has been proposed and soon became the main format in micro-FIA system [9–12]. Verpoorte and her coworkers [9] fabricated a micro-valve for sample injection and integrated both electrochemical and photometric detectors in a silica microchip for analyzing phosphate ions. Because of the difficulty in micro-valve fabrication, external pumps and injection valves instead of micro-valve fabricated on microchip were proposed. The established micro-FIA system with two external injection pumps was verified using numerical simulations [13]. Such system could also be used to determine antioxidant [14]. In this case, the injected sample volume is still very large, and the zone injection cannot be effectively achieved using the external pumps. In 1992, Manz's group [15] made a great progress in realizing non-valve sample injection in microchips using a electroosmotic

* Correspondence to: Department of Chemistry, Nanjing University, Nanjing 210093, China. Tel./fax: +86 25 83597436.
** Corresponding author. Tel./fax: +86 25 83597436.
E-mail addresses: xhxia@nju.edu.cn (X.-H. Xia), fangqun@zju.edu.cn (Q. Fang).
[1] Present address: State Key Laboratory of Microbial Resources, Institute of Microbiology, Chinese Academy of Sciences, Beijing 100101, China.

http://dx.doi.org/10.1016/j.talanta.2015.03.051
0039-9140/

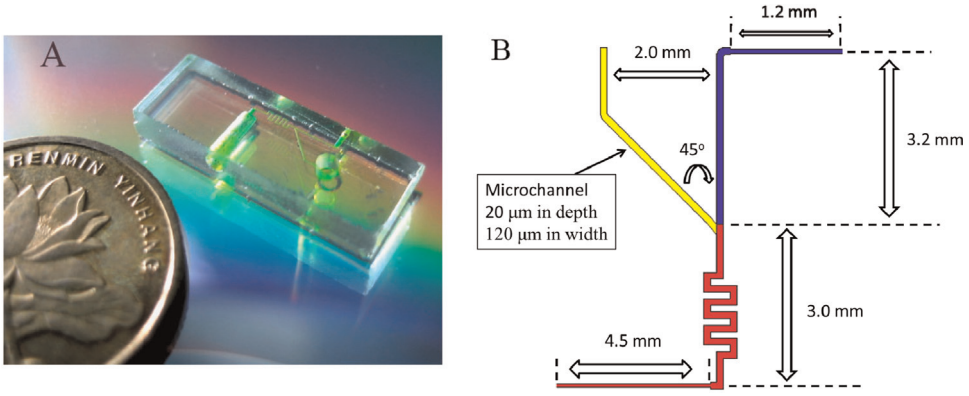

Fig. 1. Photograph of the chip used in a micro-FIA system driven by the gravity (A) and the fracture of simulation domain used in the numerical model (B). The outlet channel for controlling the difference in liquid levels is not included. The yellow and blue regions represent the sub-domains 1 and 2, respectively. These two regions are only used for introduction of reagent and sample, respectively. The red region is the sub-domain 3, where sample and reagent get mixed and then reaction starts. (For interpretation of the references to color in this figure legend, the reader is referred to the web version of this article.)

pump. However, the long-time stability of the whole system should be improved due to the Joule heat effect. This problem can be overcome simply by using the gravity driving force instead of the electroosmotic pump. We showed that gravity driven micro-FIA system could realize the zone sample injection (Fig. 1A) [16]. In this system, nanoliter sample injection and high-throughput analysis can be achieved easily.

Up to now, numerous mathematical models have been established to study the mechanism of mass transport in traditional FIA [17–24]. The "black" box method was first adopted to address mass transport in the complicated FIA systems. The regression equations [17–20] and artificial neural networks [21] are two typical representations. These methods can be used to predict reactions in FIA, however, they meet the main drawback of the requirement of a larger number of experimental data. Therefore, this "black" box method has been replaced by the analytical method in the recent years. On the basis of the mathematical descriptions of the flow pattern, mass-transport and chemical reaction kinetics, the analytical method allows deep insights into the process of FIA systems. For example, the dispersion of sample and chemical reaction kinetics can be successfully described by using the analytical methods [22–24].

With the development of photolithographic techniques, fabrication of microchip with smaller size has become feasible. It has been reported that miniaturization of the FIA systems will induce complicated mass transport behavior, i.e., the molecular diffusion will become the predominant factor in determining the chemical reaction kinetics as scaling down the dimension. Therefore, study of the interactions among diffusion, convection and chemical reaction kinetics will help us to have a comprehensive understanding of the chemical reactions in the micro-FIA systems and design appropriate micro-FIA system. In this work, a finite element model (FEM) is established to extract chemical reaction kinetics in a micro-FIA system using high throughput sample introduction. The effects of reactants diffusion, the flow velocity and injection volume on the reaction product have been simulated. The good agreement between the simulated and the experimental results demonstrates the effectiveness of the established simulation method.

2. Theory and numerical method

In the current study, the physical model for the microchip with gravity driven flow can be established by using the following equations. Firstly, the mass and momentum transports in the gravity driven flow are governed by the Navier–Stokes equation.

$$\rho\frac{\partial u}{\partial t} - \nabla\cdot\eta(\nabla u + (\nabla u)^T) + \rho u\cdot\nabla u + \nabla p = f \quad (1)$$

$$\nabla\cdot u = 0 \quad (2)$$

where, ρ is the density of fluid, η is the dynamic viscosity of fluid, and f is the body force of fluid; u is the velocity of the fluid; p is the pressure of fluid.

Since the inertial forces of the fluid are small compared to viscosity forces, $\rho u\cdot\nabla u$ can be set as zero. Furthermore, there are no applied pressure gradients, thus, Eq. (1) can be simplified into the Stokes equation.

$$\rho\frac{\partial u}{\partial t} - \nabla\cdot\eta(\nabla u + (\nabla u)^T) = f \quad (3)$$

where, f is the body force of fluid and set as $f = \rho g$.

The diffusion and convection equation accounts for the mass transport and reaction in micro-FIA system by combining with the term of chemical reaction kinetics.

$$\frac{\partial c_i}{\partial t} + \nabla\cdot(-D_i\nabla c_i + c_i u) = R_i \quad (4)$$

where, c_i and D_i denote the concentration and diffusion coefficient of species i, respectively; R denotes the reaction term, which is formulated by

$$R = kc_1c_3 \quad (5)$$

where, k is the reaction rate constant, c_1 and c_3 denote the concentrations of reaction reagent and sample, respectively. Considering that the concentration of reagent (c_1) is larger than the concentration of sample (c_3), the whole chemical reaction can be simplified into a pseudo-first-order reaction. Therefore, the reaction term R can be rewritten into $R = k'c_3$ (where $k' = k^*c_1$).

Based on Eqs. (2)–(5), the FEM model for describing the micro-FIA system is established. The whole computation domain is divided into 3 sub-domains as shown in Fig. 1B, the yellow and blue regions represent the sub-domains 1 and 2, respectively. These two regions are only used for introduction of reagent and sample. The red region is the sub-domain 3, where sample and reagent get mixed and then reaction starts. Therefore, due to no reaction in the sub-domains 1 and 2, the reaction term in Eq. (4) is not considered. The boundary and initial conditions for the FEM model are listed in Table 1.

The scales of our computation domain (Fig. 1B) are identical to the ones in experiments reported recently [16]. The injection volume of sample can be simulated by controlling the width of sample plug in numerical model. Therefore, autosample system is not necessary to be included in our numerical model.

Since the driving force in the micro-FIA system is gravity, the difference of liquid levels (10–60 cm) makes the FEM solving process difficult [16]. In this study, scales of the microchip used in our experiments are 120 μm in width and 20 μm in depth. To attain satisfied simulation results in this multi-scale model, an appropriate mesh must be considered. As we know, the precision of FEM simulation results and the computation time depend on the numbers of mesh. An appropriate mesh distribution can provide better simulations within shorter computation time, especially in the multi-scale model. Therefore, different sizes of mesh elements are adopted in the 3 sub-domains. The mesh distribution in this model is displayed in Fig. 2. In addition, back-mixing at the junction of sub-domains 1 and 2 (Fig. 1B) is hardly observed during the study of mix efficiency with different diffusion coefficients (Fig. 3A).

Hydrodynamic equations (Eqs. (2) and (3)) are first solved in stationary for acquiring the velocity profile of the micro-FIA system. Then, the time dependent solutions for the Eq. (4) are computed on the basis of velocity profile in micro-FIA system. The established FEM model and its solving process are performed in COMSOL Multiphysics 3.5a (Stockholm, Sweden). We check the influence of mesh sizes on numerical solutions by comparing the numerical solution errors at different mesh sizes. As shown in Fig. S1 (Supplementary information), the numerical solution error for the peak concentration of the final product simulated using low, moderate and high meshed size is only 3%, demonstrating that the designed mesh sizes are appropriate.

3. Experiment

3.1. Fabrication of microfluidic device

The chip with a design and scales (Fig. 1B) was fabricated using Standard photolithographic and wet chemical etching techniques. The corresponding microfluidic device was fabricated on a 1.7 mm thick 6×9 mm^2 glass plate with chromium and photoresist coat. The whole chip was bonded by using low temperature pre-bonding followed by high temperature bonding [25]. Scales of the fabricated microfluidic chip are 20 μm in depth and 120 μm in width. Detailed information on the scale of the microfluidic device is presented in Fig. 1B.

3.2. Micro-FIA system

The micro-FIA system was a microfluidic device integrated with a capillary sampling probe, reagent reservoir, and an array of microsample vials which were fixed on a home-built autosample platform modified from a chart recorder (LM14-164, Dahua Instruments, Shanghai, China) holding a tray on which fixed

Table 1
The boundary and initial conditions for the FEM model.

Computation domain	Boundary and initial conditions			
	Inlet	Outlet	Wall	
Sub-domain 1	Normal stress $p=0$ N/m^2 $c_1=2.5$ mM, $c_2=c_3=c_4=0$	$u = u_{subdomain1}$ $c_1=2.5$ mM, $c_2=c_3=c_4=0$	$u = 0$ Insulation/symmetry	Eq. (3) Eq. (4)
Sub-domain 2	Normal stress $p=0$ N/m^2 $c_1=c_4=0$, $c_2=1$ mM, $c_3=0.08$ mM	$u = u_{subdomain2}$ $c_1=c_4=0$, c_2, c_3	$u = 0$ Insulation/symmetry	Eq. (3) Eq. (4)
Sub-domain 3 $R = kc_3$ $k=2500$ s^{-1}(inital condition)	Continuity Continuity	Normal stress $p=0$ N/m^2 Continuity	$u=0$ Insulation/symmetry	Eq. (3) Eq. (4)

Note: c_i denote the concentration of species i (1 – reagent, 2 – buffer, 3 – sample, 4 – product, etc.).

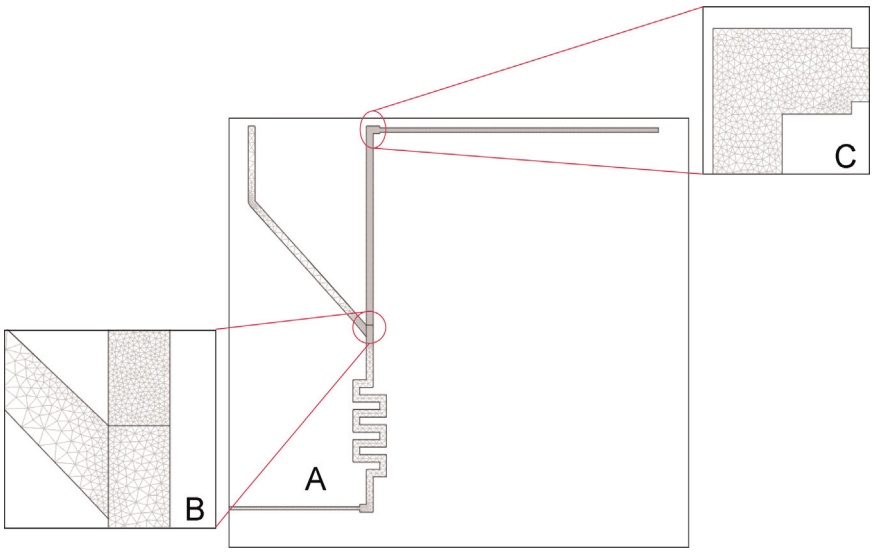

Fig. 2. Mesh distribution in the computation domain (A). Partially enlarged view for mesh distribution on the cross sub-domains 1, 2 and 3 (B), and partially enlarged view for mesh distribution on the corner of the sub-domain 2 (C).

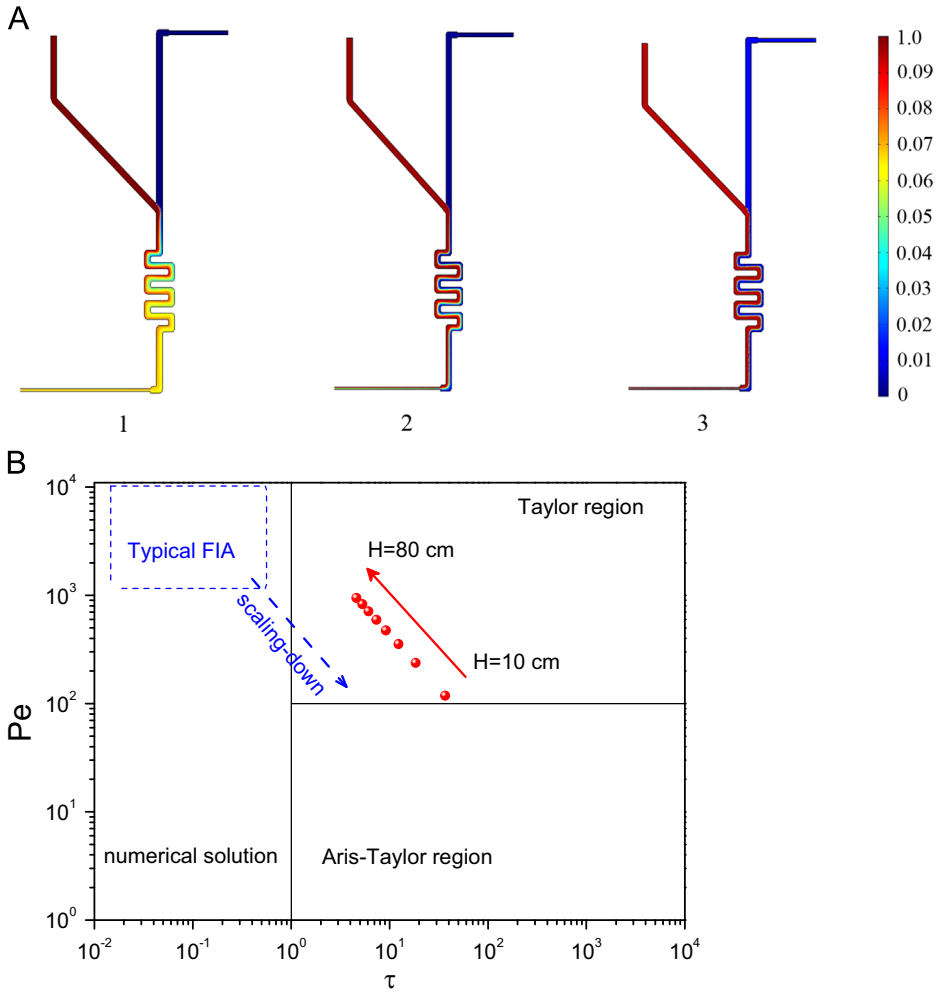

Fig. 3. (A) Numerical simulations on mixing efficiency of reagent (left channel with dimensionless concentration 0.1) with carrier/sample (right channel with dimensionless concentration 0) with different diffusion coefficients of reagent (1×10^{-9} m/s^2 (1), 1×10^{-10} m/s^2 (2), 1×10^{-11} m/s^2 (3)) and the same Reynolds number (Re=2.6) laminar flow; (B) regions of dispersion model in the micro-FIA system driven under varied liquid level difference (from 10 cm to 80 cm). (For interpretation of the references to color in this figure, the reader is referred to the web version of this article.)

positions for 30 vials were reserved. The flow of fluid was manipulated by varying the level of the waste reservoir in relation to that of the reagent reservoir/sampling probe (gravity driven flow). In experiments, series of $FeSO_4$ standard solutions in the range of 1–100 μM were used as sample (blue region of Fig. 1B); the deionized water was used as the carrier; the *o*-phenanthroline solution was pipetted into the reagent channel (yellow region of Fig. 1B).

4. Results and discussion

4.1. Sample mixing and Taylor dispersion in a micro-FIA system

The sample (sample band) and reagent (continuous flow) get mixed and then reaction starts at the junction of sample (blue region in Fig. 1B) and reagent channel (yellow region in Fig. 1B). As the laminar flow is predominant in microchannels, the contribution of diffusion becomes significant in the mixing. For attaining the best mixing efficiency on the micro-FIA structure, the numerical simulation is first used to evaluate the effect of diffusion coefficient on mixing efficiency.

The mixing efficiency with varied Peclet number (Pe) is evaluated at the same Reynolds number (Re). The Peclet number is defined by Eq. (6),

$$Pe = \frac{ud}{D} \tag{6}$$

where, d is the hydraulic diameter of the channel, u is the mean downstream velocity of a fluid with diffusion coefficient D. The Reynolds number of Re=2.6 is calculated as the ratio of the inertial to viscous forces in flow ($Re=\rho ud/\mu$, here, ρ and μ denote the density and viscosity of liquid, respectively). As shown in Fig. 3A, the reagent is diluted by carrier to 66% of its initial concentration at $Pe=2.6\times10^3$ ($D=1\times10^{-9}$ m^2 s^{-1}) (Fig. 3, A1). However, when the Pe number increases from 2.6×10^4 to 2.6×10^5, namely the diffusion coefficient becomes lower (Fig. 3A2 and A3), the reagent will be diluted to 84% and 90% of the initial concentration, respectively. As expected, the mixing efficiency drops with the decrease of diffusion coefficient. Therefore, the structure of such microchips is only suitable for small molecules mixing since macromolecules usually have smaller diffusion coefficients.

With the scaling down of the FIA systems, the relationship between Pe and the reduced time (τ) moves from the numerical solution region into the Taylor dispersion region [26]. The reduced time (τ) is defined by Eq. (7):

$$\tau = \frac{4t_v D}{d^2} \tag{7}$$

where, d is the hydraulic diameter of the channel and t_v is the residence time of the sample. In this region, peak becomes more

symmetric. Therefore, several groups have established theoretical models based on this Taylor dispersion to improve the predictability of FIA performance [26]. In the present work, Taylor's analysis of dispersion is used to characterize the micro-FIA system. The numerical solutions for dispersion at different velocities can be described by two dimensionless parameters of the Peclet number (Pe) and the reduced time (τ) [27], and the results are shown in Fig. 3B (red solid cycles). The Pe and τ in the range of different velocities (induced by the difference in liquid level from 10 to 80 cm) are then calculated. All the results (red solid cycles in Fig. 3B) are located in the Taylor region ($Pe > 100$ and $\tau > 1$) in all the used velocities, and show a linear relationship. These results clearly demonstrate that the flow conditions move from the numerical solution region to Taylor dispersion region with scaling down the FIA systems. However, it can also be observed that the flow conditions will move to the Aris–Taylor region if the flow velocity becomes lower, namely, the difference in liquid level becomes lower than 10 cm. In this case, the peak shape of the sample band will be distorted. Therefore, the calculated results are helpful in determining the experimental conditions of chemical reactions in micro-FIA systems.

Since sample dispersion is mainly caused by the convection and molecular diffusion, symmetrical Gaussian shape peak is developed in the micro-FIA system. The peak variance (σ^2_{peak}) can be described as [16]

$$\sigma^2_{peak} = \frac{d^2}{96D} t_v \tag{8}$$

This equation shows that the band-broadening of the Taylor flow increases proportionally with the residence time. Since the residence time is reciprocal to the difference in liquid level, the liquid levels in the range of 50–80 cm are used in our measurements for obtaining good band shape.

4.2. Effect of sample flow velocity and injection volume

In our measurements, the micro-FIA reaction system was composed of a reaction microchip with a capillary sampling probe, reagent reservoir, and an array of microsample vials fixed on a home-built autosampler platform as we reported previously [16]. The coordination reaction of *o*-phenanthroline with Fe(II) was chosen as a model system. The sample plugs of Fe(II) standard solutions (injected from the right channel in Fig. 1B) merged with the reagent (*o*-phenanthroline, injected from the left channel in Fig. 1B) at the reaction channel of the chip driven by gravity [16]. The amount of sample loaded could be changed by adjusting the different liquid level. Therefore, for reflecting the real state of experiment, the diffusion coefficients of *o*-phenanthroline (1×10^{-9} m^2 s^{-1}) and Fe(II) (7.19×10^{-9} m^2 s^{-1}) [28] were used in the numerical model.

The flow velocity of 10 cm liquid level difference in a FEM model is first calculated. For reducing the burden of computation, we adopt this model to simulate the other micro-FIA systems with higher differences in liquid level by multiplying the corresponding coefficients to the velocity of 10 cm differences in liquid level (channel of sample injection as reference zero point). Therefore, the same FEM model can be used for simulations by introducing different body forces into Eq. (3). The concentration profiles of chemical reaction product are obtained by averaging the concentrations over the cross section of channel as a function of flow velocities (Fig. 4).

From the results in Fig. 4, it is clear that the peak height of the reaction product increases with the increase of fluids flow rate, while the elution time decreases accordingly. The increase in peak height is due to the proportional increase in sample volume with the increase of sample loading flow rate during a fixed sampling period. The reduction in elution time is due to the proportional increase in total flow rate including those of the sample, reagent, and carrier. The simulated results demonstrate that the differences in liquid level of 60–80 cm could result in good optimal concentration profile of the reaction product (shape) in the present micro-FIA system, which is in good agreement with the observation in our previous report [16].

The effect of injected sample volume on the product peak is evaluated by using numerical simulations. The results in Fig. 5 show a typical behavior similar to that in conventional FIA systems [29]. The peak height of product increases with volume rather

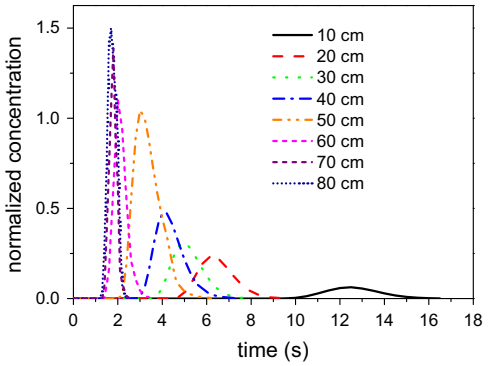

Fig. 4. The concentration profiles of the chemical reaction product as a function of fluids flow-rate (10, 20, 30, 40, 50, 60, 70 and 80 cm of difference in liquid levels between sample vial/reagent reservoir and waste reservoir). The sampling time is the same for all fluid flow rates. The concentration profiles of products are obtained by using boundary integration at the outlet of micro-FIA system and normalized using concentration of sample (0.08 mM).

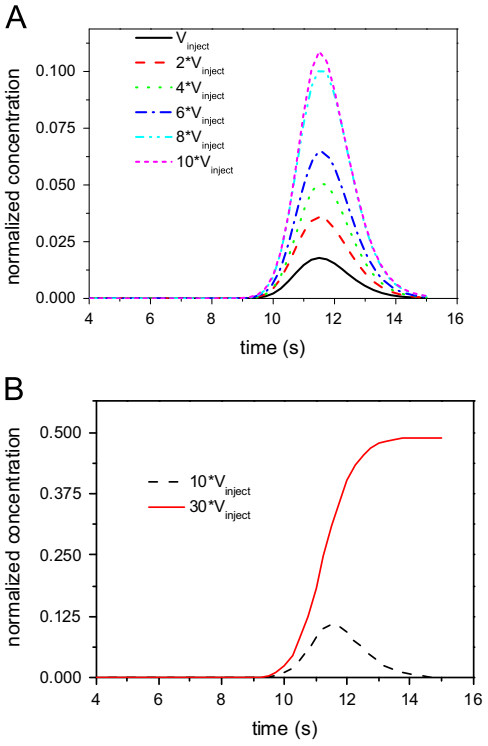

Fig. 5. The concentration profiles of reaction product with injection volumes of 1, 2, 4, 6, 8, and 10 times (A) and 30 times (B) of the initial sample injection volume at the same sampling flow-rate (10 cm difference of liquid level). V_{inject} denotes the initial sample injection volume. The concentration profiles of products are obtained by using boundary integration at the outlet of micro-FIA system and normalized using concentration of sample (0.08 mM).

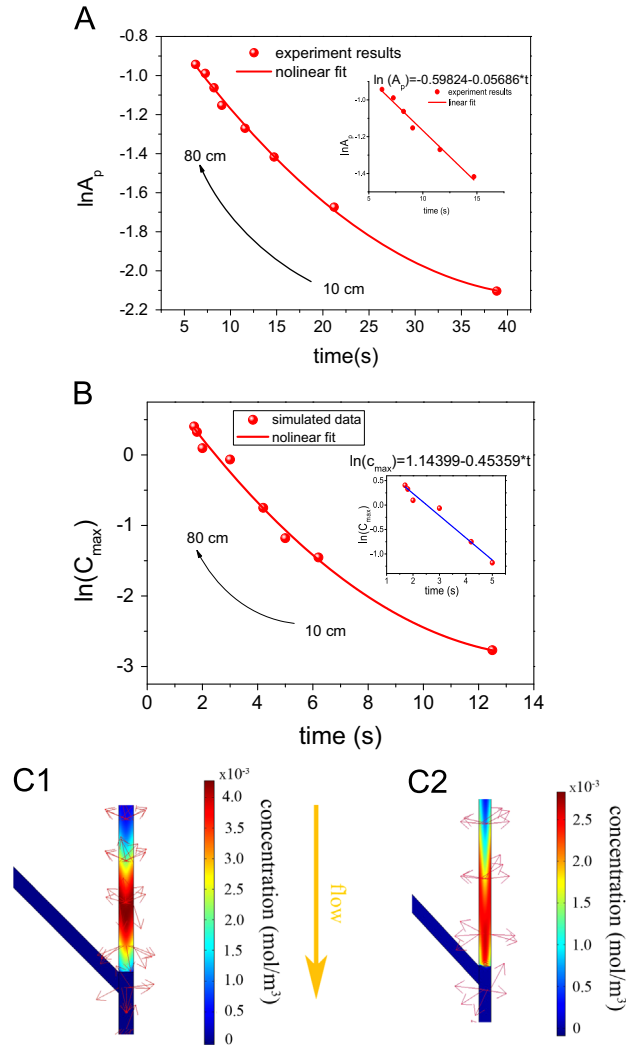

Fig. 6. (A) The plot of ln A_P against time, where A_p is the absorbance of the product formed at different velocities (experimental results adopted from ref. [16]). Inset shows the linear fit of the experimental results from 30 to 80 cm difference of liquid levels. (B) Plot of ln C_{max} against time, where C_{max} is the normalized maximum concentration of the product (Fig. 4) simulated from 10 to 80 cm difference of liquid levels. Inset shows the linear fit of the simulated results from 30 to 80 cm difference of liquid levels. (C) The diffusive fluxes of the sample plug at low velocity (C1: 10 cm difference in liquid levels, C2: 40 cm difference in liquid levels). The red arrows represent the diffusive fluxes of sample and yellow arrow represents the flow direction of the sample plug. (For interpretation of the references to color in this figure legend, the reader is referred to the web version of this article.)

rapidly when the injection volume is small. As the injection volume increases to 30 folds of the initial injection volume, the peak height of the product reaches a plateau. This result is similar to that obtained previously (the plateau was reached at 20 folds of the initial injection volume) [16]. This small difference could be due to the lower velocity simulated (0.13 cm/s) than the experimental one for each liquid level difference (0.7–0.9 cm/s), thus, more reaction products are formed because of the longer time for mixing and reaction in the numerical simulations.

Based on the experimental and simulated results, the kinetic of pseudo-first-order reaction is plotted in Fig. 6. Based on the first-order reaction law, if logarithmic scale of absorbance (ln A_p) in product is plotted against time (t), a straight line will be obtained. However, as shown in Fig. 6A, the logarithmic scales in product absorbance (ln A_p) have a nonlinear relationship with time. While results in higher differences in liquid level (30–80 cm) have a good linear relation with time (inset in Fig. 6A). Similar phenomena can be also observed from the simulated results in Fig. 6B. Experimental results can be explained if the radial diffusion is considered in microchannel at low velocities. Due to the coupling effect of radial and axial diffusions, the change in probability of collision between the sample and reagent induces a variation of the reaction apparent rate constant. Therefore, the nonlinear kinetic relationship of reaction can be attributed to coupling effect of diffusion and convection at low velocities. Especially, at low velocities, the diffusion and convection induced by the chemical reaction in the shorter channel cannot be neglected. Therefore, these two parameters alter the concentration profiles within the plug and concentration boundaries (Fig. 6C). Due to the confluence of reagents and samples, the diffusive fluxes of samples towards wall and flow direction of the fluid are larger than the ones towards interface of reagents and samples (Fig. 6C1). However, we find that with increasing the sample velocity to 40 cm difference in liquid levels, the diffusive fluxes of samples towards interface of reagents and samples apparently increase (Fig. 6C2). These results demonstrate that differences in diffusive fluxes of samples will affect the collision frequency and in turn the chemical reaction in experiments, changing the concentration of reagents and samples at the interface of confluence in the simulations. The coupling of these processes thus results in appearance of nonlinear kinetic relationship.

5. Conclusion

In summary, the interaction of mass transfer and reaction kinetics in a micro-FIA system has been investigated by using the FEM method. In the micro-FIA system, diffusion becomes the main driving force to mass transfer. The hydrodynamic behavior of micro-FIA system is still located in the Taylor diffusion region for the gravity driving forces used in this work. The concentration profiles of reaction product with different sample velocities and injection volumes are evaluated with the numerical model, which in well agreement with the results in our previous report [16]. Comparing with the conventional FIA systems, the pseudo-first-order reaction of micro-FIA displays a non-linear kinetic relationship, which may be mainly caused by the variation of apparent reaction rate and concentration at the interface of confluence flow at the induced by the co-effect of diffusion and convection. The real reason is yet to be demonstrated by further theoretical simulations and experiments. Nevertheless, the present micro-FIA system can be driven by various forces, such as gravity, electrokinetic and pressure. Therefore, various flow models can be applied into the present system for DNA analysis [30], amino acids separation [31], enzyme catalyzed reaction [32] and rapid mix [33]. The work in this manuscript provides theoretical basis for the mentioned applications.

Acknowledgments

This work was supported by grants from the National Basic Research Program (2012CB933800), the National Natural Science Foundation of China (21275070), the National Science Fund for Creative Research Groups (21121091), and the China Postdoctoral Science Foundation (2012T50483).

Appendix A. Supplementary information

Supplementary data associated with this article can be found in the online version at http://dx.doi.org/10.1016/j.talanta.2015.03.051.

References

[1] J. Ruzicka, E.H. Hansen, Anal. Chim. Acta 78 (1975) 145–157.
[2] J. Ruzicka, G.D. Marshall, Anal. Chim. Acta 237 (1990) 329–343.
[3] J. Ruzicka, Analyst 125 (2000) 1053–1060.
[4] P. Yager, T. Edwards, E. Fu, K. Helton, K. Nelson, M.R. Tam, B.H. Weigl, Nature 442 (2006) 412–418.
[5] A.J. deMello, Nature 442 (2006) 394–402.
[6] J. Kobayashi, Y. Mori, K. Okamoto, R. Akiyama, M. Ueno, T. Kitamori, S. Kobayashi, Science 304 (2004) 1305–1308.
[7] A.E. Kamholz, B.H. Weigl, B.A. Finlayson, P. Yager, Anal.Chem. 71 (1999) 5340–5347.
[8] M. Tokeshi, T. Minagawa, T. Kitamori, Anal.Chem. 72 (2000) 1711–1714.
[9] E.M.J. Verpoorte, B.H. Vanderschoot, S. Jeanneret, A. Manz, H.M. Widmer, N.F. Derooij, J. Micromech. Microeng. 4 (1994) 246–256.
[10] J.C. Fettinger, A. Manz, H. Ludi, H.M. Widmer, Sens. Actuators B 17 (1993) 19–25.
[11] E. Verpoorte, A. Manz, H. Ludi, A.E. Bruno, F. Maystre, B. Krattiger, H.M. Widmer, B.H. Vanderschoot, N.F. Derooij, Sens. Actuators B 6 (1992) 66–70.
[12] A. Manz, N. Graber, H.M. Widmer, Sens. Actuators B 1 (1990) 244–248.
[13] E.B. van Akker, M. Bos, W.E. van der Linden, Anal. Chim. Acta 373 (1998) 227–239.
[14] M. Amatatongchai, O. Hofmann, D. Nacapricha, O. Chailapakul, A.J. Demello, Anal. Bioanal. Chem. 387 (2007) 277–285.
[15] D.J. Harrison, A. Manz, Z.H. Fan, H. Ludi, H.M. Widmer, Anal. Chem. 64 (1992) 1926–1932.
[16] W.B. Du, Q. Fang, Q.H. He, Z.L. Fang, Anal. Chem. 77 (2005) 1330–1337.
[17] Y. Narusawa, Y. Miyamae, Anal. Chim. Acta 309 (1995) 227–239.
[18] Y. Narusawa, Y. Miyamae, Anal. Chim. Acta 296 (1994) 129–140.
[19] M. Delvalle, M. Poch, J. Alonso, J. Bartroli, Anal. Chim. Acta 241 (1990) 31–42.
[20] J. Ruzicka, E.H. Hansen, E.A. Zagatto, Anal. Chim. Acta 88 (1977) 1–16.
[21] M. Hartnett, D. Diamond, P.G. Barker, Analyst 118 (1993) 347–354.
[22] V.P. Andreev, M.I. Khidekel, Anal. Chim. Acta 278 (1993) 307–316.
[23] H. Wada, S. Hiraoka, A. Yuchi, G. Nakagawa, Anal. Chim. Acta 179 (1986) 181–188.
[24] C.C. Painton, H.A. Mottola, Anal. Chim. Acta 158 (1984) 67–84.
[25] Z.J. Jia, Q. Fang, Z.L. Fang, Anal.Chem. 76 (2004) 5597–5602.
[26] G.I. Taylor, Proc. R. Soc. Lond. 1137 (1953) 186–203.
[27] W.E. Vanderlinden, Trends Anal. Chem. 6 (1987) 37–40.
[28] David R. Lide, CRC Handbook of Chemistry and Physics, 82nd edition, C.R.C. Press, New York, 2002.
[29] J.M. Reijn, W.E. Vanderlinden, H. Poppe, Anal. Chim. Acta 114 (1980) 105–118.
[30] X.-F. Fan, Q. Li, S.-L. Wang, Z.-R. Xu, W.-B. Du, Q. Fang, Z.-L. Fang, Electrophoresis 29 (2008) 4733–4738.
[31] Q.-H. He, Q. Fang, W.-B. Du, Z.-L. Fang, Electrophoresis 28 (2007) 2912–2919.
[32] Y. Li, D. Zhang, X. Feng, Y. Xu, B.-F. Liu, Talanta 88 (2012) 175–180.
[33] K. Malecha, L.J. Golonka, J. Baldyga, M. Jasinska, P. Sobieszuk, Sens. Actuators B 143 (2009) 400–413.